Chemical Science

RSC Publishing

EDGE ARTICLE

View Article Online
View Journal | View Issue

Mononuclear nickel(II)-superoxo and nickel(III)-peroxo complexes bearing a common macrocyclic TMC ligand†

Cite this: *Chem. Sci.*, 2013, **4**, 1502

Jaeheung Cho,‡[ab] Hye Yeon Kang,‡[a] Lei V. Liu,[c] Ritimukta Sarangi,[d] Edward I. Solomon[cd] and Wonwoo Nam*[a]

Mononuclear metal-dioxygen adducts, such as metal-superoxo and -peroxo species, are generated as key intermediates in the catalytic cycles of dioxygen activation by heme and non-heme metalloenzymes. We have shown recently that the geometric and electronic structure of the Ni–O_2 core in $[Ni(n\text{-TMC})(O_2)]^+$ (n = 12 and 14) varies depending on the ring size of the supporting TMC ligand. In this study, mononuclear Ni(II)-superoxo and Ni(III)-peroxo complexes bearing a common macrocylic 13-TMC ligand, such as $[Ni^{II}(13\text{-TMC})(O_2)]^+$ and $[Ni^{III}(13\text{-TMC})(O_2)]^+$, were synthesized in the reaction of $[Ni^{II}(13\text{-TMC})(CH_3CN)]^{2+}$ and H_2O_2 in the presence of tetramethylammonium hydroxide (TMAH) and triethylamine (TEA), respectively. The Ni(II)-superoxo and Ni(III)-peroxo complexes bearing the common 13-TMC ligand were successfully characterized by various spectroscopic methods, X-ray crystallography and DFT calculations. Based on the combined experimental and theoretical studies, we conclude that the superoxo ligand in $[Ni^{II}(13\text{-TMC})(O_2)]^+$ is bound in an end-on fashion to the nickel(II) center, whereas the peroxo ligand in $[Ni^{III}(13\text{-TMC})(O_2)]^+$ is bound in a side-on fashion to the nickel(III) center. Reactivity studies performed with the Ni(II)-superoxo and Ni(III)-peroxo complexes toward organic substrates reveal that the former possesses an electrophilic character, whereas the latter is an active oxidant in nucleophilic reaction.

Received 7th December 2012
Accepted 9th January 2013

DOI: 10.1039/c3sc22173c

www.rsc.org/chemicalscience

Published on 11 January 2013 on http://pubs.rsc.org | doi:10.1039/C3SC22173C
Downloaded by Ewha Womens University on 05 March 2013

Introduction

Mononuclear metal–dioxygen species (M–O_2) have been implicated as key intermediates in the catalytic cycles of dioxygen activation by heme and non-heme metalloenzymes.[1] A number of metal complexes binding an O_2 unit, such as metal-superoxo and -peroxo species, have been synthesized as chemical models of the M–O_2 intermediates,[2] and the binding modes of the O_2 unit (*e.g.*, end-on (η^1) *vs.* side-on (η^2) and superoxo *vs.* peroxo) and the electronic nature of metal ions in the synthetic M–O_2 complexes have been intensively investigated with various spectroscopic methods and X-ray crystallography.[3] The reactivity of M–O_2 complexes in electrophilic and nucleophilic reactions has also been the subject of intense scrutiny. For example, side-on synthetic iron(III)-peroxo complexes with heme and non-heme ligands have been structurally and spectroscopically characterized and investigated in oxidative nucleophilic reactions (*e.g.*, aldehyde deformylation).[4,5] As biomimetic compounds of copper-containing enzymes, a number of synthetic side-on and end-on copper(II)-superoxo and side-on copper(III)-peroxo complexes have been structurally and spectroscopically characterized and investigated in oxidative electrophilic reactions.[6] It was also shown that the electronic nature of the copper–O_2 core (*e.g.*, copper(II)-superoxo *vs.* copper(III)-peroxo) varies depending on the supporting ligands of the copper complexes.[3b,7]

Recently, we have reported the synthesis, spectroscopic and structural characterization and reactivities of metal complexes with O_2-derived ligands bearing *N*-tetramethylated cyclam (TMC) chelates.[8] In these studies, the ring size of the TMC ligands is shown to be an important factor in regulating the geometric and electronic structures of the M–O_2 complexes (*e.g.*, side-on $M^{(n+1)+}$-peroxo *vs.* end-on M^{n+}-superoxo).[9,10] One notable example is the finding that a side-on Ni(III)-peroxo complex is formed with a 12-TMC ligand (Scheme 1, blue-colored species),[9b] whereas 14-TMC ligand affords an end-on Ni(II)-superoxo complex (Scheme 1, red-colored species).[9a] Similarly, the formation of an end-on Cr(III)-superoxo complex and a side-on Cr(IV)-peroxo complex has been reported in the reactions of $[Cr^{II}(14\text{-TMC})]^{2+}$ and $[Cr^{II}(12\text{-TMC})]^{2+}$ with O_2, respectively.[10]

[a]*Department of Bioinspired Science, Ewha Womans University, Seoul 120–750, Korea. E-mail: wwnam@ewha.ac.kr; Fax: +82 2-3277-4441; Tel: +82 2-3277-2392*

[b]*Department of Emerging Materials Science, DGIST, Daegu 711-873, Korea*

[c]*Department of Chemistry, Stanford University, Stanford, California 94305, USA*

[d]*Stanford Synchrotron Radiation Lightsource, SLAC National Accelerator Laboratory, Stanford University, Menlo Park, California 94025-7015, USA*

† Electronic supplementary information (ESI) available: Synthesis and characterization data and kinetic details. CCDC reference numbers 729199 and 900983. For ESI and crystallographic data in CIF or other electronic format see DOI: 10.1039/c3sc22173c

‡ These authors contributed equally to this work.

This journal is © The Royal Society of Chemistry 2013

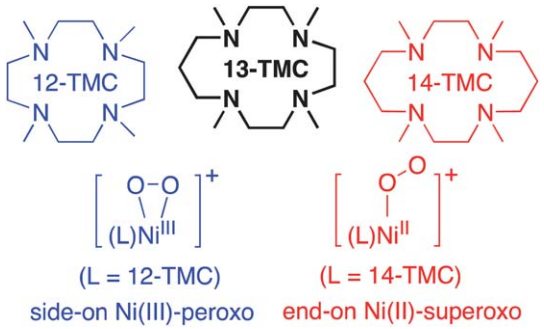

Scheme 1 A schematic drawing showing the effect of the ring-size of macrocyclic TMC ligands on the formation of Ni–O_2 intermediates; 12-TMC, 1,4,7,10-tetramethyl-1,4,7,10-tetraazacyclododecane; 13-TMC, 1,4,7,10-tetramethyl-1,4,7,10-tetraazacyclotridecane; 14-TMC, 1,4,8,11-tetramethyl-1,4,8,11-tetraazacyclotetradecane.

Published on 11 January 2013 on http://pubs.rsc.org | doi:10.1039/C3SC22173C
Downloaded by Ewha Womens University on 05 March 2013

As our ongoing efforts to elucidate the ring size effect of TMC ligands on the geometric and electronic structure of the Ni–O_2 core in $[Ni(n\text{-TMC})(O_2)]^+$ (n = 12–14), we synthesized $[Ni(13\text{-TMC})(O_2)]^+$ and compared its structure with those of the previously reported $[Ni^{III}(12\text{-TMC})(O_2)]^+$ and $[Ni^{II}(14\text{-TMC})(O_2)]^+$ complexes (see Scheme 1). Interestingly, we observed the formation of two different intermediates, an end-on Ni(II)-superoxo complex (**2**, $[Ni^{II}(13\text{-TMC})(O_2)]^+$) and a side-on Ni(III)-peroxo complex (**3**, $[Ni^{III}(13\text{-TMC})(O_2)]^+$), depending on the base used in the reaction (Scheme 2, reaction *a* with tetramethylammonium hydroxide (TMAH) and reaction *b* with triethylamine (TEA)).[11] These Ni(II)-superoxo and Ni(III)-peroxo complexes bearing a common 13-TMC ligand were characterized with various spectroscopic methods and X-ray crystallography, and their reactivities were compared in electrophilic and nucleophilic reactions.

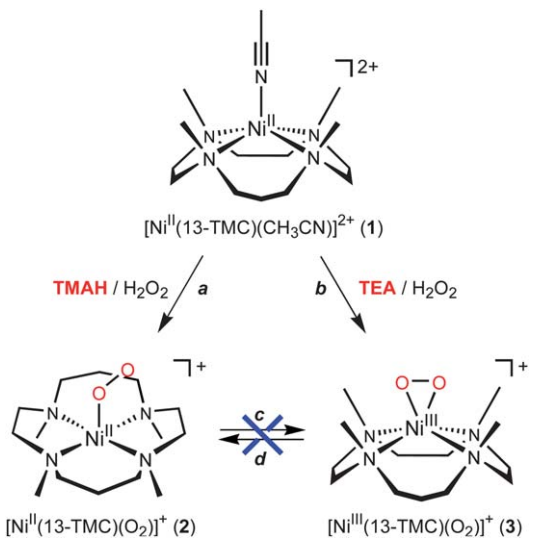

Scheme 2 Synthetic routes for the preparation of **2** and **3**. The structure of the end-on Ni(II)-superoxo complex (**2**) was drawn based on the crystal structure of an end-on Cr(III)-superoxo complex, $[Cr^{III}(O_2)(14\text{-TMC})]^{2+}$.[10a]

Results and discussion

Synthetic procedures for Ni–O_2 complexes bearing a 13-TMC ligand are depicted in Scheme 2. The starting material, $[Ni^{II}(13\text{-TMC})(CH_3CN)]^{2+}$ (**1**), was prepared by reacting $Ni(ClO_4)_2\cdot 6H_2O$ and 13-TMC in CH_3CN under an inert atmosphere and characterized with various spectroscopic methods, such as UV-vis absorption spectroscopy, electrospray ionization mass spectrometry (ESI-MS) and X-ray crystallography (see ESI, Experimental section, Fig. S1–S3, Tables S1 and S2†).

Complex **2** was prepared by adding 2 equiv. of H_2O_2 to a reaction solution containing **1** in the presence of 1.3 equiv. of TMAH in CH_3CN at –40 °C (Scheme 2, reaction *a*); the color of the solution changed from purple to yellowish green. A UV-vis spectrum of **2** shows an intense band at 339 nm (ε = 800 M^{-1} cm^{-1}) and two weak bands at 416 nm (ε = 130 M^{-1} cm^{-1}) and 684 nm (ε = 60 M^{-1} cm^{-1}) (Fig. 1a), which is similar to that of the previously reported nickel(II)-superoxo complex bearing a 14-TMC ligand, $[Ni^{II}(14\text{-TMC})(O_2)]^+$ (see Fig. 1a).[9a] Although we were not able to obtain an ESI-MS of **2** due to its thermal instability, the

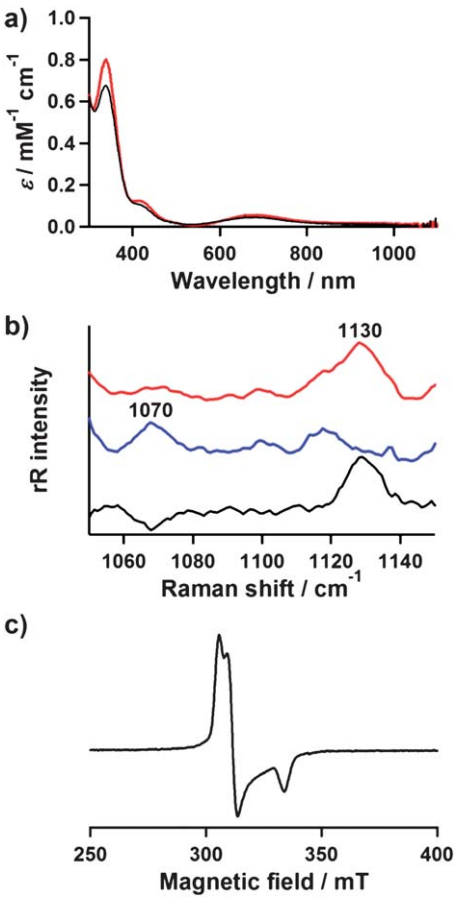

Fig. 1 (a) UV-vis spectra of $[Ni^{II}(13\text{-TMC})(O_2)]^+$ (**2**) (red line) and $[Ni^{II}(14\text{-TMC})(O_2)]^+$ (black line) in CH_3CN at –40 °C. (b) Resonance-Raman spectra of **2** (16 mM) obtained upon excitation at 458 nm at 77 K; **2** prepared with $H_2{}^{16}O_2$ (red line) and $H_2{}^{18}O_2$ (blue line). The black line shows the difference of the spectra prepared with $H_2{}^{16}O_2$ and $H_2{}^{18}O_2$. (c) X-Band EPR spectrum of **2** in frozen CH_3CN at 5 K. Instrumental parameters: microwave power = 0.989 mW, frequency = 9.646 GHz, sweep width = 0.25 T, modulation amplitude = 1 mT.

Published on 11 January 2013 on http://pubs.rsc.org | doi:10.1039/C3SC22173C
Downloaded by Ewha Womens University on 05 March 2013

resonance-Raman spectrum of **2** was successfully collected using 413 nm excitation in CH_3CN at 77 K (Fig. 1b). **2** prepared with $H_2{}^{16}O_2$ exhibits an isotopically sensitive band at 1130 cm^{-1}, which shifts to 1070 cm^{-1} when $H_2{}^{18}O_2$ is used. The observed isotopic shift of –60 cm^{-1} with ^{18}O-substitution is in agreement with the calculated value ($\Delta\nu_{calc} = -64$ cm^{-1}) for the O–O diatomic harmonic oscillator. The observed O–O frequency at 1130 cm^{-1} is comparable to those reported for end-on metal-superoxo complexes bearing 14-TMC, such as $[Ni^{II}(14\text{-TMC})(O_2)]^+$ (1131 cm^{-1})[9a] and $[Cr^{III}(14\text{-TMC})(O_2)(Cl)]^+$ (1170 cm^{-1}),[10a] indicating the superoxo character of the O_2 unit in **2**. The electron paramagnetic resonance (EPR) spectrum of a frozen CH_3CN solution of **2** at 5 K exhibits a rhombic signal with *g* values of 2.25, 2.21 and 2.06 (Fig. 1c), which is a typical $(d_{z^2})^1$ electron configuration observed for Ni(II)-superoxo[9a,12] and Ni(III) complexes.[13]

Interestingly, when the reaction was performed in the presence of TEA instead of TMAH, a different species was produced (Scheme 2, reaction *b*). The reaction of **1** with 10 equiv. of H_2O_2 in the presence of 2 equiv. of TEA in CH_3CN at 10 °C produces a green intermediate **3**, which shows distinct absorption features that are different from those of **2** but similar to those of the recently reported nickel(III)-peroxo complex bearing 12-TMC, $[Ni^{III}(12\text{-TMC})(O_2)]^+$ (Fig. 2a). The ESI-MS of **3** exhibits a prominent signal at a mass-to-charge (*m*/*z*) ratio of 332.0 (Fig. 2b), whose mass and isotope distribution pattern correspond to $[Ni(13\text{-TMC})(O_2)]^+$ (calculated *m*/*z* 332.2) (Fig. 2b, inset). When **3** was prepared with isotopically labelled $H_2{}^{18}O_2$, the mass peak corresponding to **3** shifted to *m*/*z* 336.0 (Fig. 2b, inset). The shift in four mass units upon substitution of ^{16}O with ^{18}O indicates that **3** contains an O_2 unit. On 458 nm excitation at 77 K, the resonance-Raman spectrum of ^{16}O-labelled **3** in CH_3CN shows an isotopically sensitive band at 1008 cm^{-1}, which shifts to 950 cm^{-1} on ^{18}O-substitution (Fig. 2c). The O–O stretch of **3** is lower than those of Ni(II)-superoxo complexes, such as **2** (1130 cm^{-1}) and $[Ni^{II}(14\text{-TMC})(O_2)]^+$ (1131 cm^{-1}),[9a] but similar to that of the Ni(III)-peroxo complex, $[Ni^{III}(12\text{-TMC})(O_2)]^+$ (1002 cm^{-1}).[9b] The EPR spectrum of a frozen CH_3CN solution of **3** measured at 5 K exhibits an axial signal with *g* values of 2.19 and 2.07 (Fig. 2d). The room-temperature magnetic moment of 2.1 μ_B, determined using the ^1H NMR Evans method,[14] is consistent with an $S = 1/2$ ground state.

The single-crystal structure of **3** revealed the mononuclear side-on Ni-peroxo complex in a distorted octahedral geometry (Fig. 3). The O–O bond length (1.383(4) Å) of **3** is comparable to that of $[Ni^{III}(12\text{-TMC})(O_2)]^+$ (1.386 Å). In addition, a good correlation was observed when the O–O bond length and O–O stretching frequency of **3** was fitted in the plot of O–O stretching frequency *vs.* O–O bond length for side-on metal-O_2 complexes (ESI, Fig. S4†).[3,8] Based on the X-ray crystallography and spectroscopic data, **3** is assigned unambiguously as a side-on Ni(III)-peroxo complex.

Ni K-edge XAS data on **2** and **3** are presented in Fig. 4. The inset shows the expanded pre-edge region. The pre-edge features arise due to electric dipole-forbidden quadrupole-allowed 1s → 3d transitions.[15] The pre-edge for **2** and **3** is at 8331.6 and 8332.3 eV, respectively (ESI, Table S3†). The ~0.7 eV shift reflects a significant increase in ligand field in **3** relative to **2**, attributable to the side-on (η^2) binding of O_2 in **3**, in contrast to the end-on (η^1) binding expected in **2**. To higher energy is the intense, dipole-allowed 1s → 4p + continuum transitions. A shift in the rising-edge to high energies indicates an increase in oxidation state. For Ni compounds, typically, a small shift in edge energies is observed with oxidation.[16] The rising-edge for **2** and **3** is at 8331.4 and 8331.7 eV, respectively, consistent with their respective Ni^{II} and Ni^{III} assignment.

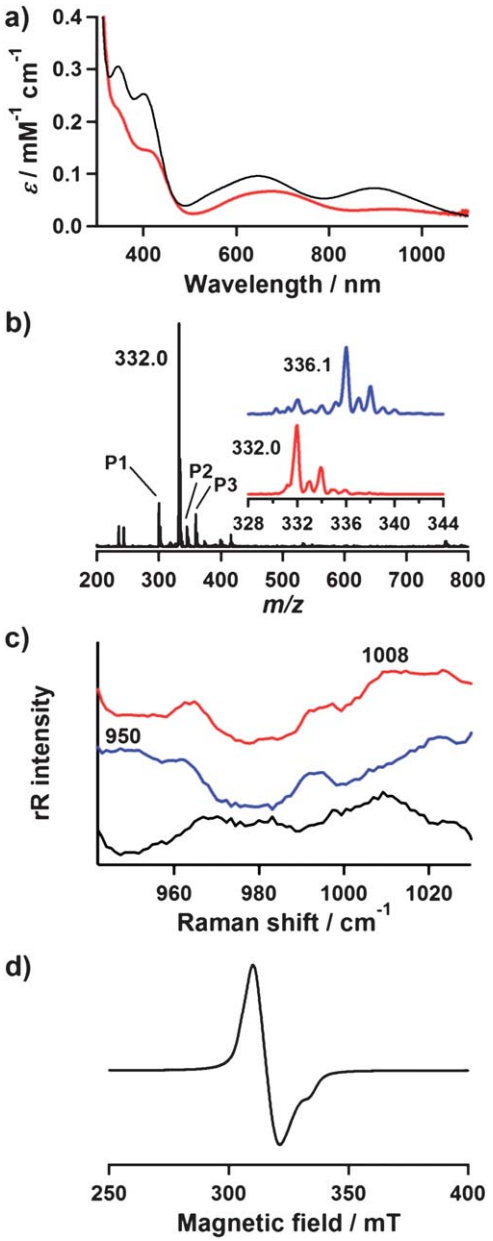

Fig. 2 (a) UV-vis spectra of $[Ni^{III}(13\text{-TMC})(O_2)]^+$ (**3**) (red line) and $[Ni^{III}(12\text{-TMC})(O_2)]^+$ (black line) in CH_3CN at 10 °C. (b) ESI-MS of **3** in CH_3CN at 10 °C. The minor peaks at *m*/*z* 300.0 (P1), 345.0 (P2) and 359.0 (P3) are assignable to $[Ni(13\text{-TMC})]^+$, $[Ni(13\text{-TMC})(HCOO)]^+$ and $[Ni(13\text{-TMC})(CH_3COO)]^+$, respectively. Insets show the observed isotope distribution patterns for $[Ni(13\text{-TMC})(^{16}O_2)]^+$ (lower) and $[Ni(13\text{-TMC})(^{18}O_2)]^+$ (upper). (c) Resonance-Raman spectra of **3** (16 mM) obtained upon excitation at 458 nm at 77 K; **3** prepared with $H_2{}^{16}O_2$ (red line) and $H_2{}^{18}O_2$ (blue line). The black line shows the difference of the spectra prepared with $H_2{}^{16}O_2$ and $H_2{}^{18}O_2$. (d) X-Band EPR spectrum of **3** in frozen CH_3CN at 5 K. Instrumental parameters: microwave power = 1.013 mW, frequency = 9.646 GHz, sweep width = 0.25 T, modulation amplitude = 1 mT.

This journal is © The Royal Society of Chemistry 2013

Published on 11 January 2013 on http://pubs.rsc.org | doi:10.1039/C3SC22173C
Downloaded by Ewha Womens University on 05 March 2013

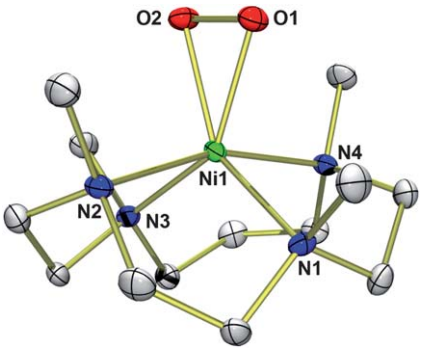

Fig. 3 ORTEP plot of $[Ni^{III}(13\text{-TMC})(O_2)]^+$ (**3**) with 30% probability thermal ellipsoids. Hydrogen atoms are omitted for clarity. Selected bond lengths (Å) and angles (°): Ni–O1 1.897(3), Ni–O2 1.898(3), Ni–N1 2.046(3), Ni–N2 2.192(3), Ni–N3 2.076(3), Ni–N4 2.210(3), O1–O2 1.383(4); O1–Ni–O2 42.73(12), Ni–O1–O2 68.369(16), Ni–O2–O1 68.58(16).

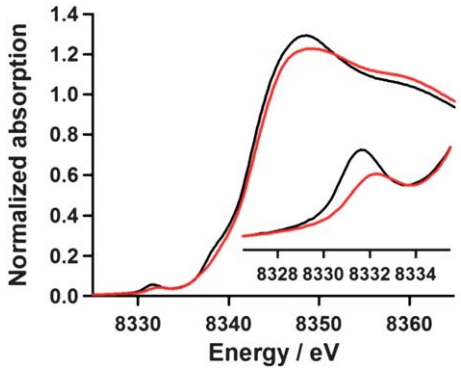

Fig. 4 Normalized Ni K-edge X-ray absorption spectra for **2** (black line) and **3** (red line). The inset shows the expanded pre-edge region.

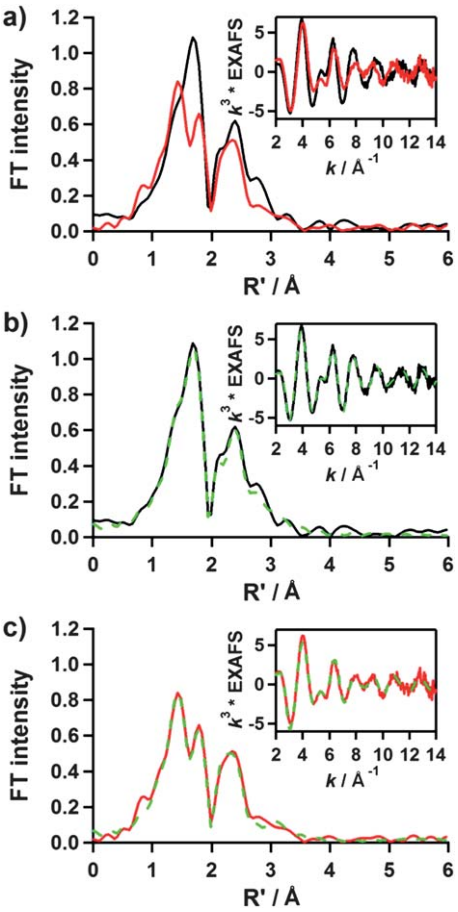

Fig. 5 (a) Comparison of the nonphase-shift corrected Fourier-transforms (FT) for **2** (black line) and **3** (red line). The inset shows the corresponding EXAFS data. FEFF best-fit results for **2** and **3** are shown in (b) and (c), respectively; data (solid line) and fit (dashed line).

The non-phase shift corrected Fourier transforms and the corresponding EXAFS data for **2** and **3** are presented in Fig. 5a. Their respective FEFF fits are presented in Fig. 5b and c and ESI, Tables S4 and S5.† The data show a large change in the first shell between **2** and **3**. The first shell of **2** is fit with 1 Ni–O at 1.91 Å and 5 Ni–N at 2.10 Å. A three shell fit with 1 Ni–O at 1.90 Å, 4 Ni–N at 2.07 Å and 1 Ni–N at 2.17 Å is also consistent with the data (Fig. 5b); this supports an end-on (η^1) O_2 binding in **2**. The presence of a sixth ligand could indicate *trans*-axial Ni–N(MeCN) ligation. The first shell of **3** is fit with 2 Ni–O at 1.89 Å, 2 Ni–N at 2.05 Å and 2 Ni–N at 2.16 Å (Fig. 5c), which is in excellent agreement with the crystal structure. Thus, the large difference in the first shells between **2** and **3** reflects the presence of the additional short Ni–O bond in **3**.

Density functional theory (DFT) calculations were performed to evaluate the geometric and electronic structures of **2** and **3**. The calculated metrical and electronic parameters of **3** are consistent with the experimental data presented here and support the side-on (η^2) bound Ni^{III}-peroxide complex (ESI, Table S6†). DFT calculations of **2** show 1 short Ni–O distance at 1.95 Å and 4 longer Ni–N distances at ~2.13 Å. No evidence of a *trans* axial CH_3CN ligation was found, although EXAFS data indicate the presence of a weakly bound sixth ligand. The Mulliken spin density analysis indicates two unpaired spin-up electrons on Ni and one unpaired spin-down electron on O_2 indicating a Ni^{II} (d^8, $S = 1$) antiferromagnetically coupled with an O_2^- ($S = 1/2$) system, resulting in the d_{z^2} doublet ground state in **2**. These results are consistent with the end-on (η^1) bound Ni^{II}-superoxo assignment of **2**. The calculated O–O bond distance for **2** is 1.32 Å, while that of **3** is 1.39 Å. This increase in O–O bond distance is typical on going from superoxo to peroxo complexes.

Finally, it is of interest to note that interconversion between **2** and **3** does not occur. This is surprising since DFT calculations show that interconversion energy is low (~3 kcal mol^{-1}; see ESI, Fig. S5†). For example, since the only difference in the synthetic procedures for the generation of **2** and **3** was the base (*e.g.*, TMAH for **2** and TEA for **3**, as shown in Scheme 2), we added TEA and TMAH to the solutions of **2** and **3** after these intermediates were generated. In these reactions, we did not observe the interconversion between them (Scheme 2, reactions *c* and *d*). One plausible explanation for no interconversion between **2** and **3** is that the *N*-methyl groups in **2** and **3** have a different orientation in the superoxo and peroxo moieties (*e.g.*, *anti* to the superoxo moiety in **2** *vs. syn* to the peroxo moiety in **3**, as

Published on 11 January 2013 on http://pubs.rsc.org | doi:10.1039/C3SC22173C
Downloaded by Ewha Womens University on 05 March 2013

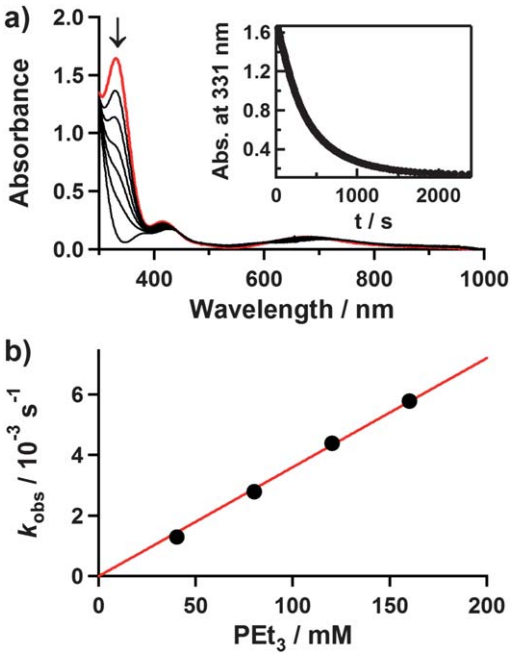

Fig. 6 Reactions of $[Ni^{II}(13\text{-TMC})(O_2)]^+$ (**2**) with PEt_3 in CH_3CN–CH_3OH (1 : 1) at –40 °C. (a) UV-vis spectral changes of **2** (2 mM) upon addition of 40 equiv. of PEt_3. Inset shows the time course of the absorbance at 331 nm. (b) Plot of k_{obs} against PEt_3 concentration to determine a second-order rate constant.

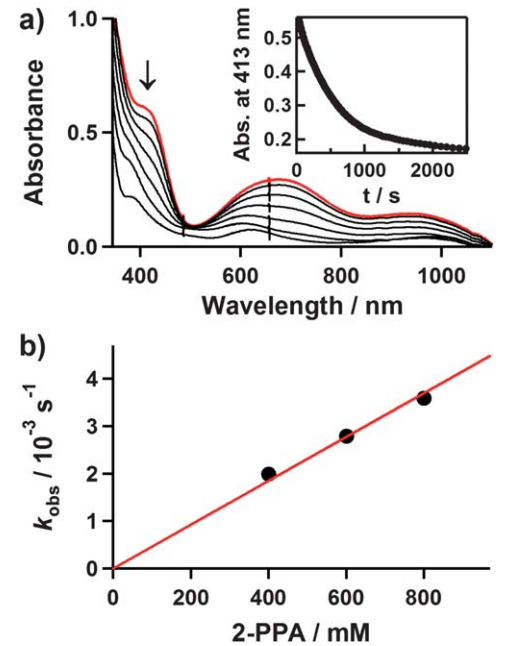

Fig. 7 Reactions of $[Ni^{III}(13\text{-TMC})(O_2)]^+$ (**3**) with 2-PPA in CH_3CN at 25 °C. (a) UV-vis spectral changes of **3** (4 mM) upon addition of 100 equiv. of 2-PPA. Inset shows the time course of the absorbance at 413 nm. (b) Plot of k_{obs} against 2-PPA concentration to determine a second-order rate constant.

proposed in Scheme 2). This is consistent with known crystal structures of metal-superoxo and -peroxo complexes bearing TMC ligands.[8] *N*-methyl groups in the Cr-superoxo complex are oriented *anti* to the superoxo group,[10a] whereas those in the metal-peroxo complexes are pointed *syn* to the peroxo moiety.[5a,10c,17] In contrast to this theory, DFT calculations show that the *anti* structure of **2** is energetically unfavorable (ESI, Table S7†). An alternative possibility, based on the EXAFS data, is the presence of a sixth ligand (a solvent, MeCN, water or OH^- (from TMAH)), which ligates axially to the Ni in **2** and precludes the interconversion; however, DFT calculations do not support *trans*-axial coordination in **2**. Nonetheless, the role of the bases for the formation of different Ni–O_2 intermediates is not clear at this moment and remains elusive.

We then examined the reactivities of **2** and **3** in oxidative electrophilic and nucleophilic reactions. Since it has been shown that metal-superoxo species are active oxidants in electrophilic reactions,[6,9a,10a,18] the reactivity of **2** was first investigated in the oxidation of triethylphosphine (PEt_3) in CH_3CN–CH_3OH (1 : 1) at –40 °C. As shown in Fig. 6a, the characteristic UV-vis absorption band of **2** disappeared with a pseudo-first-order decay, and product analysis of the reaction solution revealed the formation of $OPEt_3$ in a quantitative yield. The pseudo-first-order rate constants increased proportionally with the increase of the concentration of PEt_3 (Fig. 6b), giving a second-order rate constant (k_2) of 3.6×10^{-2} M^{-1} s^{-1} at –40 °C.

Unlike **2**, addition of PEt_3 to a solution of **3** in CH_3CN–CH_3OH (1 : 1) at 25 °C did not show any UV-vis spectral changes, and product analysis of the reaction solution did not reveal oxygenated products. These results indicate that **3** is not capable of conducting oxidative electrophilic reaction under the reaction conditions. In contrast, **3** is capable of deformylating aldehyde *via* nucleophilic reaction, as frequently observed in aldehyde deformylation reactions by metal-peroxo complexes.[4b,9b,17] Kinetic studies of **3** with 2-phenylpropionaldehyde (2-PPA) in CH_3CN at 25 °C show a first-order decay profile (Fig. 7a), and the pseudo-first-order rate constants increased proportionally with the aldehyde concentration ($k_2 = 4.2 \times 10^{-3}$ M^{-1} s^{-1} at 25 °C) (Fig. 7b). Product analysis of the final reaction mixture revealed the formation of acetophenone (85 ± 10%).

Conclusions

Comparisons of the structure and reactivity of metal–O_2 complexes (*i.e.*, metal-superoxo *vs.* metal-peroxo species) are of importance in understanding intrinsic properties of these intermediates in dioxygen activation and oxidation chemistry. Although we have reported recently the synthesis of metal-superoxo and -peroxo complexes by changing the ring size of the supporting TMC ligands (*e.g.*, $[Ni(n\text{-TMC})(O_2)]^+$ and $[Cr(n\text{-TMC})(O_2)]^+$ with n = 12 and 14),[9,10] the synthesis of metal-superoxo and -peroxo complexes bearing a common TMC ligand has not been shown previously. In this work, we have shown the first successful synthesis of an end-on Ni(II)-superoxo complex, $[Ni^{II}(13\text{-TMC})(O_2)]^+$ (**2**), and a side-on Ni(III)-peroxo complex, $[Ni^{III}(13\text{-TMC})(O_2)]^+$ (**3**), bearing a common macrocyclic 13-TMC ligand. These intermediates were fully characterized with various spectroscopic techniques, X-ray crystallography and DFT calculations. In particular, resonance-Raman spectroscopy together with EXAFS clearly differentiates an end-on bound superoxo ligand of **2** (*e.g.*, ν(O–O) of

 This journal is © The Royal Society of Chemistry 2013

Published on 11 January 2013 on http://pubs.rsc.org | doi:10.1039/C3SC22173C
Downloaded by Ewha Womens University on 05 March 2013

1130 cm^{-1}) and a side-on bound peroxo ligand of **3** (*e.g.*, ν(O–O) of 1008 cm^{-1}). The reactivities of **2** and **3** were also compared in electrophilic and nucleophilic reactions; **2** is capable of conducting oxidative electrophilic reaction, whereas **3** shows no electrophilic reactivity but is an active oxidant in nucleophilic reaction. Although we were successful in generating Ni(II)-superoxo and Ni(III)-peroxo complexes bearing a common supporting ligand in the presence of two different bases, the role of the bases and the exact mechanism of the formation of two different Ni–O_2 intermediates in the reactions of Ni(II) complex and H_2O_2 is not known at this moment and will be the subject of future studies.

Experimental section

Generation and characterization of $[Ni^{II}(13\text{-TMC})(O_2)]^+$ (2)

Treatment of $[Ni^{II}(13\text{-TMC})(CH_3CN)](ClO_4)_2$ (**1**, 2 mM) with 2 equiv. of H_2O_2 in the presence of 1.3 equiv. of TMAH in CH_3CN at –40 °C afforded the formation of a yellowish green solution. Spectroscopic data, including UV-vis, resonance-Raman and EPR, are reported in Fig. 1. $[Ni^{II}(13\text{-TMC})(^{18}O_2)]^+$ was prepared by adding 2 equiv. of $H_2{}^{18}O_2$ (14 μL, 90% ^{18}O-enriched, 2% $H_2{}^{18}O_2$ in water) in the presence of 1.3 equiv. of TMAH in CH_3CN (2 mL) at –40 °C.

Generation and characterization of $[Ni^{III}(13\text{-TMC})(O_2)]^+$ (3)

Treatment of **1** (4 mM) with 10 equiv. of H_2O_2 in the presence of 2 equiv. of triethylamine (TEA) in CH_3CN (2 mL) afforded the formation of a green solution at 25 °C. Spectroscopic data, including UV-vis, ESI-MS, resonance-Raman and EPR, were reported in Fig. 2. $[Ni^{III}(13\text{-TMC})(^{18}O_2)]^+$ was prepared by adding 10 equiv. of $H_2{}^{18}O_2$ (138 μL, 90% ^{18}O-enriched, 2% $H_2{}^{18}O_2$ in water) to a solution containing **1** (4 mM) and 2 equiv. of TEA in CH_3CN (2 mL) at ambient temperature. Crystals suitable for X-ray crystallography were obtained by slow diffusion of Et_2O into a solution of **3** in CH_3CN.

Reactivity studies

All reactions were run monitoring UV-vis spectral changes of reaction solutions, and rate constants were determined by fitting the changes in absorbance at 331 nm for $[Ni^{II}(13\text{-TMC})(O_2)]^+$ (**2**) and 413 nm for $[Ni^{III}(13\text{-TMC})(O_2)]^+$ (**3**). Reactions were run at least in triplicate, and the data reported represent the average of these reactions. *In situ*-generated **2** and **3** were used in kinetic studies, such as the oxidation of PEt_3 in CH_3CN–CH_3OH (1 : 1) at –40 °C and 2-PPA in CH_3CN at 25 °C, respectively. After completion of the reactions, pseudo-first-order fitting of the kinetic data allowed us to determine k_{obs} values. Products formed in the oxidation of PEt_3 by **2** in CH_3CN–CH_3OH (1 : 1) at –40 °C were analyzed by ^{31}P and ^{1}H NMR spectroscopy; $OPEt_3$ was formed as a sole product in the oxidation of PEt_3 by **2**. Products formed in the oxidation of 2-PPA by **3** in CH_3CN at 25 °C were analyzed by injecting the reaction mixture directly into GC and GC-MS; acetophenone (85 ± 10%) was the sole product detected in this reaction.

X-Ray crystallography

Crystal data for $1(ClO_4)_2$. $C_{15}Cl_2NiN_5O_8$, tetragonal, *P*4/*nmm*, $Z = 2$, $a = 9.2584(6)$, $b = 9.2584(6)$, $c = 14.1473(17)$ Å, $V = 1212.68(18)$ Å^3, $\mu = 1.065$ mm^{-1}, $D_c = 1.391$ g cm^{-3}, $R_1 = 0.0612$, $wR_2 = 0.1594$ for 912 unique reflections, 75 variables. CCDC reference number 729199.

Crystal data for $3(ClO_4)\cdot CH_3CN$. $C_{15}H_{33}ClNiN_5O_6$, monoclinic, *Pc*, $Z = 2$, $a = 7.7299(2)$, $b = 7.7263(2)$, $c = 17.8514(5)$ Å, $\beta = 100.673(2)°$, $V = 1047.70(5)$ Å^3, $\mu = 1.095$ mm^{-1}, $D_c = 1.501$ g cm^{-3}, $R_1 = 0.0360$, $wR_2 = 0.0762$ for 3604 unique reflections, 258 variables. CCDC reference number 900983.

Acknowledgements

W. N. at EWU acknowledges the financial support from the NRF/MEST of Korea through the CRI, GRL (2010-00353) and WCU (R31-2008-00-10010-0) and the 2011 KRICT OASIS Project. The research at DGIST was supported by the DGIST R & D program of the Ministry of Education, Science and Technology, Korea (J. C.). E. I. S. at Stanford University acknowledges the financial support from NIH grants (GM 40392 and DK 031450). XAS data were measured at the Stanford Synchrotron Radiation Lightsource (SSRL), SSRL operations are funded by the Department of Energy, Office of Basic Energy Sciences. The SSRL Structural Molecular Biology program is supported by the National Institutes of Health (NIH), National Institute of General Medical Sciences and the National Center for Research Resources, Biomedical Technology Program; and the Department of Energy, Office of Biological and Environmental Research. This publication was made possible by Grant Numbers P41GM103393 and P41RR001209 from the NIH. Its contents are solely the responsibility of the authors and do not necessarily represent the official view of NIGMS, NCRR or NIH.

Notes and references

1 W. Nam, *Acc. Chem. Res.*, 2007, **40**, 465, and review articles in the special issue.
2 (*a*) S. Yao and M. Driess, *Acc. Chem. Res.*, 2012, **45**, 276–287; (*b*) A. Bakac, *Coord. Chem. Rev.*, 2006, **250**, 2046–2058; (*c*) M. Costas, M. P. Mehn, M. P. Jensen and L. Que, Jr, *Chem. Rev.*, 2004, **104**, 939–986; (*d*) L. M. Mirica, X. Ottenwaelder and T. D. P. Stack, *Chem. Rev.*, 2004, **104**, 939–986; (*e*) E. I. Solomon, T. C. Brunold, M. I. Davis, J. N. Kemsley, S.-K. Lee, N. Lehnert, F. Neese, A. J. Skulan, Y.-S. Yang and J. Zhou, *Chem. Rev.*, 2000, **100**, 235–349; (*f*) I. M. Klotz and D. M. Kurtz, Jr, *Chem. Rev.*, 1994, **94**, 567–568, and review articles in the special issue.
3 (*a*) C. J. Cramer, W. B. Tolman, K. H. Theopold and A. L. Rheingold, *Proc. Natl. Acad. Sci. U. S. A.*, 2003, **100**, 3635–3640; (*b*) C. J. Cramer and W. B. Tolman, *Acc. Chem. Res.*, 2007, **40**, 601–608.
4 (*a*) T. Ohta, J.-G. Liu and Y. Naruta, *Coord. Chem. Rev.*, 2013, **257**, 407–413; (*b*) D. L. Wertz and J. S. Valentine, *Struct. Bonding*, 2000, **97**, 37–60.
5 (*a*) J. Cho, S. Jeon, S. A. Wilson, L. V. Liu, E. A. Kang, J. J. Braymer, M. H. Lim, B. Hedman, K. O. Hodgson,

Published on 11 January 2013 on http://pubs.rsc.org | doi:10.1039/C3SC22173C
Downloaded by Ewha Womens University on 05 March 2013

J. S. Valentine, E. I. Solomon and W. Nam, *Nature*, 2011, **478**, 502–505; (*b*) J.-J. Girerd, F. Banse and A. J. Simaan, *Struct. Bonding*, 2000, **97**, 145–177; (*c*) F. Neese and E. I. Solomon, *J. Am. Chem. Soc.*, 1998, **120**, 12829–12848.

6 (*a*) P. Chen and E. I. Solomon, *Proc. Natl. Acad. Sci. U. S. A.*, 2004, **101**, 13105–13110; (*b*) S. Itoh, *Curr. Opin. Chem. Biol.*, 2006, **10**, 115–122; (*c*) M. Rolff and F. Tuczek, *Angew. Chem., Int. Ed.*, 2008, **47**, 2344–2347; (*d*) R. A. Himes and K. D. Karlin, *Curr. Opin. Chem. Biol.*, 2009, **13**, 119–131; (*e*) A. Kunishita, M. Kubo, H. Sugimoto, T. Ogura, K. Sato, T. Takui and S. Itoh, *J. Am. Chem. Soc.*, 2009, **131**, 2788–2789; (*f*) J. S. Woertink, L. Tian, D. Maiti, H. R. Lucas, R. A. Himes, K. D. Karlin, F. Neese, C. Würtele, M. C. Holthausen, E. Bill, J. Sundermeyer, S. Schindler and E. I. Solomon, *Inorg. Chem.*, 2010, **49**, 9450–9459; (*g*) R. L. Peterson, R. A. Himes, H. Kotani, T. Suenobu, L. Tian, M. A. Siegler, E. I. Solomon, S. Fukuzumi and K. D. Karlin, *J. Am. Chem. Soc.*, 2011, **133**, 1702–1705; (*h*) A. Kunishita, M. Z. Ertem, Y. Okubo, T. Tano, H. Sugimoto, K. Ohkubo, N. Fujieda, S. Fukuzumi, C. J. Cramer and S. Itoh, *Inorg. Chem.*, 2012, **51**, 9465–9480.

7 (*a*) B. F. Gherman and C. J. Cramer, *Inorg. Chem.*, 2004, **43**, 7281–7283; (*b*) R. Sarangi, N. Aboelella, K. Fujisawa, W. B. Tolman, B. Hedman, K. O. Hodgson and E. I. Solomon, *J. Am. Chem. Soc.*, 2006, **128**, 8286–8296.

8 J. Cho, R. Sarangi and W. Nam, *Acc. Chem. Res.*, 2012, **45**, 1321–1330.

9 (*a*) N. T. Kieber-Emmons, J. Annaraj, M. S. Seo, K. M. Van Heuvelen, T. Tosha, T. Kitagawa, T. C. Brunold, W. Nam and C. G. Riordan, *J. Am. Chem. Soc.*, 2006, **128**, 14230–14231; (*b*) J. Cho, R. Sarangi, J. Annaraj, S. Y. Kim, M. Kubo, T. Ogura, E. I. Solomon and W. Nam, *Nat. Chem.*, 2009, **1**, 568–572; (*c*) R. Sarangi, J. Cho, W. Nam and E. I. Solomon, *Inorg. Chem.*, 2011, **50**, 614–620.

10 (*a*) J. Cho, J. Woo and W. Nam, *J. Am. Chem. Soc.*, 2010, **132**, 5958–5959; (*b*) J. Cho, J. Woo, J. E. Han, M. Kubo, T. Ogura and W. Nam, *Chem. Sci.*, 2011, **2**, 2057–2062; (*c*) A. Yokoyama, J. E. Han, J. Cho, M. Kubo, T. Ogura, M. A. Siegler, K. D. Karlin and W. Nam, *J. Am. Chem. Soc.*, 2012, **134**, 15269–15272.

11 Irrespective of the kind of bases (*e.g.*, TMAH and TEA), 14-TMC produced an end-on Ni(II)-supeoxo species $[Ni^{II}(O_2)(14\text{-TMC})]^+$, whereas 12-TMC yielded a side-on Ni(III)-peroxo species $[Ni^{III}(O_2)(12\text{-TMC})]^+$.

12 (*a*) M. T. Kieber-Emmons and C. G. Riordan, *Acc. Chem. Res.*, 2007, **40**, 618–625; (*b*) K. Fujita, R. Schenker, W. Gu, T. C. Brunold, S. P. Cramer and C. G. Riordan, *Inorg. Chem.*, 2004, **43**, 3324–3326; (*c*) J. Cho, H. Furutachi, S. Fujinami, T. Tosha, H. Ohtsu, O. Ikeda, A. Suzuki, M. Nomura, T. Uruga, H. Tanida, T. Kawai, K. Tanaka, T. Kitagawa and M. Suzuki, *Inorg. Chem.*, 2006, **45**, 2873–2885; (*d*) S. Yao, E. Bill, C. Milsmann, K. Wieghardt and M. Driess, *Angew. Chem., Int. Ed.*, 2008, **47**, 7110–7113.

13 R. I. Haines and A. McAuley, *Coord. Chem. Rev.*, 1981, **39**, 77–119.

14 D. F. Evans and D. A. Jakubovic, *J. Chem. Soc., Dalton Trans.*, 1988, 2927–2933.

15 T. E. Westre, P. Kennepohl, J. G. DeWitt, B. Hedman, K. O. Hodgson and E. I. Solomon, *J. Am. Chem. Soc.*, 1997, **119**, 6297–6314.

16 G. J. Colpas, M. J. Maroney, C. Bagyinka, M. Kumar, W. S. Willis, S. L. Suib, N. Baidya and P. K. Mascharak, *Inorg. Chem.*, 1991, **30**, 920–928.

17 (*a*) M. S. Seo, J. Y. Kim, J. Annaraj, Y. Kim, Y.-M. Lee, S.-J. Kim, J. Kim and W. Nam, *Angew. Chem., Int. Ed.*, 2007, **46**, 377–380; (*b*) J. Annaraj, J. Cho, Y.-M. Lee, S. Y. Kim, R. Latifi, S. P. de Visser and W. Nam, *Angew. Chem., Int. Ed.*, 2009, **48**, 4150–4153; (*c*) J. Cho, R. Sarangi, H. Y. Kang, J. Y. Lee, M. Kubo, T. Ogura, E. I. Solomon and W. Nam, *J. Am. Chem. Soc.*, 2010, **132**, 16977–16986.

18 Mononuclear non-heme iron(III)-superoxo species have been proposed as active oxidants in electrophilic reactions by enzymes and biomimetic compounds: (*a*) W. A. van der Donk, C. Krebs and J. M. Bollinger, Jr, *Curr. Opin. Struct. Biol.*, 2010, **20**, 673–683; (*b*) P. C. A. Bruijnincx, G. van Koten and R. J. M. Klein Gebbink, *Chem. Soc. Rev.*, 2008, **37**, 2716–2744; (*c*) J. M. Bollinger, Jr and C. Krebs, *Curr. Opin. Chem. Biol.*, 2007, **11**, 151–158; (*d*) Y.-M. Lee, S. Hong, Y. Morimoto, W. Shin, S. Fukuzumi and W. Nam, *J. Am. Chem. Soc.*, 2010, **132**, 10668–10670; (*e*) L. W. Chung, X. Li, H. Hirao and K. Morokuma, *J. Am. Chem. Soc.*, 2011, **133**, 20076–20079; (*f*) K.-B. Cho, H. Chen, D. Janardanan, S. P. de Visser, S. Shaik and W. Nam, *Chem. Commun.*, 2012, **48**, 2189–2191.

 This journal is © The Royal Society of Chemistry 2013